Spectrochimica Acta Part A: Molecular and Biomolecular Spectroscopy 120 (2014) 445–455

Contents lists available at ScienceDirect

Spectrochimica Acta Part A: Molecular and Biomolecular Spectroscopy

journal homepage: www.elsevier.com/locate/saa

Vibrational spectroscopic (FT-IR, FT-Raman) and quantum chemical calculations of 1-(5,5-dioxido-10H-phenothiazin-10-yl)ethanone

Manpreet Kaur [a], Y. Shyma Mary [b], C. Yohannan Panicker [c,*], Hema Tresa Varghese [d], H.S. Yathirajan [a], K. Byrappa [e], Christian Van Alsenoy [f]

[a] Department of Studies in Chemistry, University of Mysore, Manasagangotri, Mysore, India
[b] Department of Physics, Bharathiar University, Coimbatore, Tamilnadu, India
[c] Department of Physics, TKM College of Arts and Science, Kollam, Kerala, India
[d] Department of Physics, Fatima Mata National College, Kollam, Kerala, India
[e] Materials Science Center, University of Mysore, NCHS Building, Manasgangotri, Mysore, India
[f] Department of Chemistry, University of Antwerp, B2610 Antwerp, Belgium

HIGHLIGHTS

- IR, Raman spectra and NBO analysis were reported.
- The wavenumbers are calculated theoretically using Gaussian09 software.
- The wavenumbers are assigned using PED analysis.
- The geometrical parameters are in agreement with that XRD data.

GRAPHICAL ABSTRACT

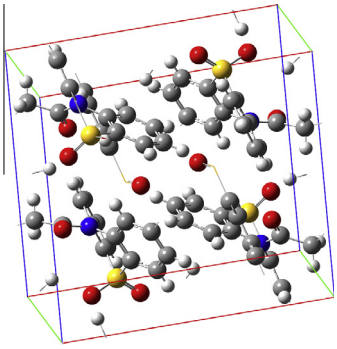

ARTICLE INFO

Article history:
Received 23 August 2013
Received in revised form 5 October 2013
Accepted 8 October 2013
Available online 17 October 2013

Keywords:
Phenothiazine
DFT
FT-IR
FT-Raman
Hyperpolarizability
MEP

ABSTRACT

FT-IR and FT-Raman spectra of 1-(5,5-dioxido-10H-phenothiazin-10-yl)ethanone were recorded and analyzed. The vibrational wavenumbers were computed using B3LYP/6-31G* and SDD basis. Potential energy distribution of normal modes of vibrations was done using GAR2PED program. The HOMO and LUMO analysis is used to determine the charge transfer within the molecule. The stability of the molecule arising from hyper conjugative interaction and charge delocalization has been analyzed using NBO analysis. Molecular electrostatic potential was performed by the DFT method and infrared intensities and Raman activities are also reported. MEP shows that the negative potential sites are on oxygen atoms and the positive potential sites are around the nitrogen atoms. The geometrical parameters of the title compound (SDD) are in agreement with XRD crystal structure data. The calculated first hyperpolarizability is comparable with the reported values of similar derivatives and is an attractive object for future studies of nonlinear optics.

Introduction

Phenothiazine is a well known heterocycle. The phenothiazine structure occurs in many synthetic dyes, electroluminescent materials [1] and drugs, especially various antipsychotic drugs, e.g. chloropromazine and antihistaminic, e.g. promethizine [2]. Recently, researchers have found some new applications for phenothiazine derivatives in medicine related to anti-tubercular [3] and antitumor activities [4]. Phenothiazines are biologically active tri-cyclic compounds containing N and S as donor atoms. Drugs based on this ring system are widely used in medicine [5–8] and chemical modifications on phenothiazine ring system has led to

* Corresponding author. Tel.: +91 9895370968.
E-mail address: cyphyp@rediffmail.com (C.Y. Panicker).

1386-1425/$ - see front matter © 2013 Elsevier B.V. All rights reserved.
http://dx.doi.org/10.1016/j.saa.2013.10.032

the discovery of drugs exhibiting various activities like neuroleptics, tranquilizers, anticholinergics, antihistaminics, anthelmintics, antiallergics, anticarcinogenics [9], anti-inflammatory agents, antibacterials, anticonvulsants [10] and as cannabinoid receptor agonists [11]. The variety of the therapeutic activities believed to be due to the presence of a fold in the heterocyclic ring along the nitrogen–sulfur axis and so phenothiazine ring system is an essential template in medicinal chemistry research and most of these phenothiazine drugs are its N-alkyl derivatives. Chlorpromazine and ethopropazine are two such derivatives which are used to treat the diseases of the central nervous system including schizophrenia [12] and tremor [13,14]. Phenothiazines substituted in the 2 and 10 positions are used in analytical chemistry as reagents in spectro photometric [15] and kinetic–catalytic determination of metals [16,17]. Bacu et al. [18] reported the synthesis of potential drug delivery systems from maleic anhydride copolymers and phenothiazine derivatives. The structure-activity relationship for inhibition of human cholinesterases by alkyl amide phenothiazine derivatives have been reported [19–21]. The ability of phenothiazines to form well defined ion-association products with certain organic compounds and metal complexes forms the basis of utilizing its binary and ternary complexes in chemical and pharmaceutical analysis. Phenothiazines are also reported to form co-ordination complexes with transition metals [22–32] and the charge transfer complexes with organic acceptors [33]. Recently phenothiazine derivatives with high electron donating properties [34] are attracting research interest due to their potential applications in material science. The ground state intra-molecular charge transfer and excited state photo-induced electron transfer properties of phenothiazine [35,36] make them serve as electro active and photoactive materials in molecular electronics. Hence they are widely used in industry as organic light emitting diodes [37,38], acid–base dyes and pigments [39], semiconductors [37], chemical sensors [40], efficient nonlinear optical materials [41] and solar cells [42]. The title compound has been used in the synthesis of oxomemazine, an antihistamine and anticholinergic drug of the phenothiazine chemical class used for the treatment of coughs. The crystal structures of dioxopromethazinium picrate [43] and 1-(10H-phenothiazin-2-yl)ethanone [44] have been reported. In the present study, IR and Raman spectra of 1-(5,5-dioxido-10H-phenothiazin-10-yl)ethanone are reported both experimentally and theoretically. The energies, degrees of hybridization, populations of the lone electron pairs of oxygen, energies of their interaction with the anti-bonding orbital of the benzene ring and the electron density distributions and $E(2)$ energies have been calculated by NBO analysis using DFT method to give clear evidence of stabilization originating from the hyper conjugation of various intra molecular interactions. There has been growing interest in using organic materials for nonlinear optical devices, functioning as second harmonic generators, frequency converters, electro-optical modulators etc. because of the large second order electric susceptibilities of organic materials. Since the second order electric susceptibility is related to first hyperpolarizability, the search for organic chromophores with large first hyperpolarizability is fully justified.

Experimental

The title compound was obtained as a gift sample from RL Fine Chem., Bangalore, India. X-ray quality crystals were obtained by slow evaporation of solution of a 1:1 mixture of acetone:ethanol. The crystal and molecular structure studies of the title compound were reported earlier [45]. In the title compound, $C_{14}H_{11}NO_3S$, the six member thiazine ring fused to two benzene rings adopts a distorted boat conformation. The crystal packing is stabilized by weak intermolecular C—H···O interactions. The ORTEP and crystal packing diagrams are given in Figs. 1 and 2. The FT-IR spectrum (Fig. 3) was recorded using KBr pellets on a DR/Jasco FT-IR 6300 spectrometer. The FT-Raman spectrum (Fig. 4) was obtained on a Bruker RFS 100/s, Germany. For excitation of the spectra the emission of Nd:YAG laser was used, excitation wavelength 1064 nm.

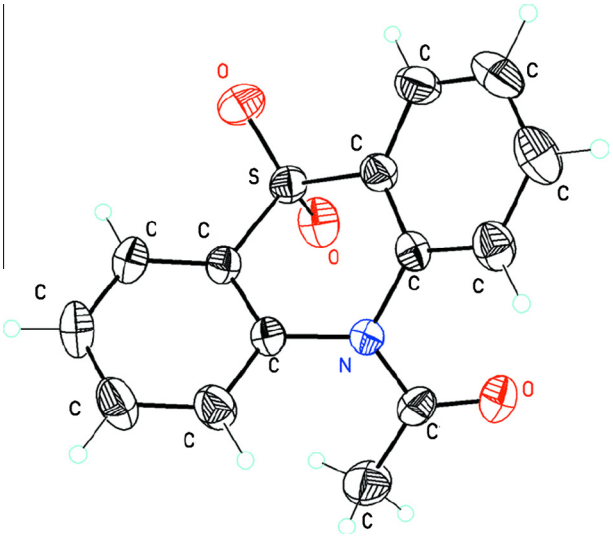

Fig. 1. ORTEP diagram of 1-(5,5-dioxido-10H-phenothiazin-10-yl)ethanone.

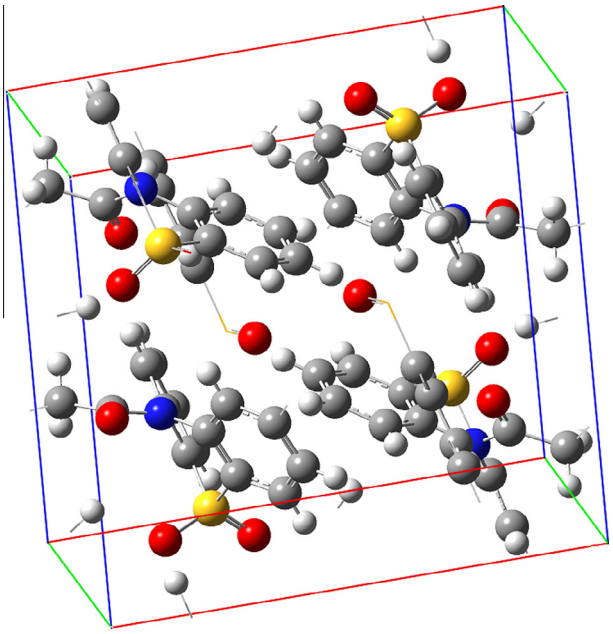

Fig. 2. Crystal packing of 1-(5,5-dioxido-10H-phenothiazin-10-yl)ethanone.

Computational details

Calculations of the title compound are carried out with Gaussian09 program [46] using the B3LYP/6-31G* and SDD basis sets to predict the molecular structure and vibrational wavenumbers. The DFT hybrid B3LYP functional and SDD methods tend to overestimate the fundamental modes; therefore scaling factor of 0.9613 has to be used for obtaining a considerably better agreement with experimental data [47]. The Stuttgard/Dresden effective core potential basis set (SDD) [48] was chosen particularly because of its advantage of doing faster calculations with relatively better

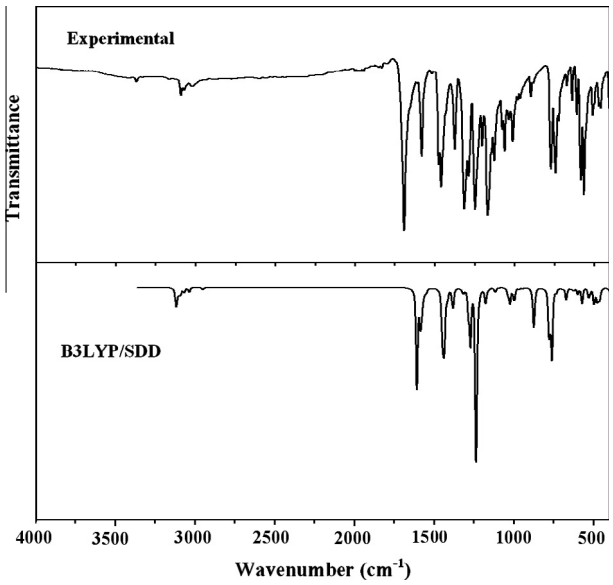

Fig. 3. FT-IR spectrum of 1-(5,5-dioxido-10H-phenothiazin-10-yl)ethanone.

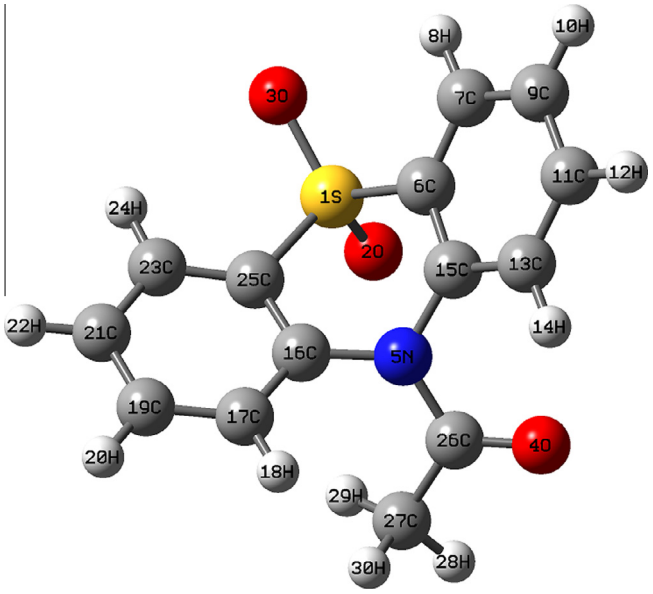

Fig. 5. Optimized geometry (SDD) of 1-(5,5-dioxido-10H-phenothiazin-10-yl)ethanone.

accuracy and structures [49]. Then frequency calculations were employed to confirm the structure as minimum points in energy. Parameters corresponding to optimized geometry (SDD) of the title compound (Fig. 5) with XRD data are given as supporting material in Table S1. The absence of imaginary wavenumbers on the calculated vibrational spectrum confirms that the structure deduced corresponds to minimum energy. The assignments of the calculated wave numbers are aided by the animation option of GAUSSVIEW program, which gives a visual presentation of the vibrational modes [50]. The first hyperpolarizability of this novel molecular system is calculated using SDD method, based on the finite field approach. In the presence of an applied electric field, the energy of a system is a function of the electric field. The natural bond orbital (NBO) calculations were performed using NBO 3.1 program [51] as implemented in the Gaussian09 package at the SDD level in order to understand various second-order interactions between the filled orbital of one subsystem and vacant orbital of another subsystem. The potential energy distribution (PED) is calculated with the help of GAR2PED software package [52].

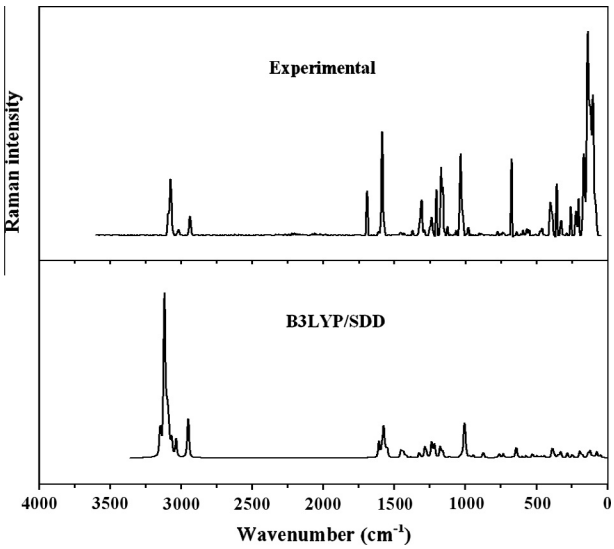

Fig. 4. FT-Raman spectrum of 1-(5,5-dioxido-10H-phenothiazin-10-yl)ethanone.

Results and discussion

IR and Raman spectra

The observed IR and Raman bands as well as calculated (scaled) wavenumbers and assignments are given in Table 1. The carbonyl stretching C=O vibration [53,54] is expected in the region 1715–1680 cm^{-1} and in the present study this mode appears at 1694 cm^{-1} in the IR spectrum and at 1693 cm^{-1} in the Raman spectrum. The SDD calculations give this mode at 1672 cm^{-1}. The deviation of the calculated wave number for this mode can be attributed to the under estimation of the large degree of their π-electron delocalization due to conjugation of the molecule [55]. The intensity of the carbonyl group vibration can increase because of conjugation or formation of hydrogen bonds. The δC=O in-plane deformation and the out-of-plane deformation γC=O are expected in the regions 625 ± 70 and 540 ± 80 cm^{-1} respectively [53]. The band observed at 638, 588 cm^{-1} in the IR and 638, 595 cm^{-1} in Raman spectrum are assigned as C=O deformation modes. The theoretically calculated values are 642 and 598 cm^{-1}. Bieliauskas et al. [56] reported the C=O stretching mode 1674 cm^{-1} for derivatives derived from phenothiazine.

The stretching vibrations of CH_3 are expected in the range 2900–3050 cm^{-1} [53,57]. The first of these result from asymmetric stretching $\upsilon_{as}CH_3$ modes in which two C—H bonds of the methyl group are extending while the third one is contracting and the other result from symmetric stretching $\upsilon_s CH_3$ in which all three of the C—H bonds extend and contract in-phase. The asymmetric stretching modes of methyl group are calculated to be at 3066, 3035 cm^{-1} and the symmetric mode at 2950 cm^{-1}. The bands at 3072, 3028 cm^{-1} in the IR spectrum and at 3074, 3025, 2955 cm^{-1} in the Raman spectrum of the title compound are assigned as the CH_3 stretching vibrations. Two bending can occur within a methyl group. The first of these, the symmetrical bending vibration, involves out-of-phase bending of the C—H bonds. The asymmetric deformations are expected in the range 1400–1485 cm^{-1} [53]. The calculated values of $\delta_{as}CH_3$ modes are at

Table 1
Vibrational assignments of 1-(5,5-dioxido-10H-phenothiazin-10-yl)ethanone.

B3LYP/6-31G*			B3LYP/SDD			IR	Raman assignments	
υ	IR_I	R_A	υ	IR_I	R_A			
3139	0.40	75.39	3147	0.61	93.92	–	–	υCHII(95)
3103	4.72	295.59	3119	16.51	296.30	–	–	υCHI(99)
3102	11.19	77.09	3116	18.44	202.75	–	–	υCHII(97)
3098	5.17	65.69	3107	4.03	46.80	–	–	υCHI(99)
3089	12.92	187.75	3100	4.46	69.00	–	–	υCHII(98)
3089	11.51	122.14	3097	6.70	56.49	3095	3091	υCHI(99)
3075	5.08	64.80	3087	5.94	50.87	–	3091	υCHII(78)
3075	2.08	74.99	3085	3.16	37.80	–	–	υCHI(95)
3055	6.09	77.43	3066	8.89	55.71	3072	3074	$\upsilon_{as}CH_3$(100)
3024	4.36	49.80	3035	7.40	46.45	3028	3025	$\upsilon_{as}CH_3$(99)
2958	2.89	107.47	2950	4.12	133.70	–	2955	$\upsilon_{s}CH_3$(79)
1727	263.77	16.54	1672	174.39	29.90	1694	1693	υC=O(60)
1590	11.42	14.29	1585	81.71	27.11	1581	1584	υPhII(59), υPhI(16)
1580	32.34	58.63	1573	25.34	56.69	1581	1584	υPhII(21), υPhI(63)
1574	16.44	24.20	1559	5.68	8.56	–	–	υPhII(19), υPhI(58)
1564	1.82	6.03	1550	6.46	17.25	–	–	υPhII(60), υPhI(23)
1464	49.77	0.75	1452	18.24	13.10	1462	1456	$\delta_{as}CH_3$(91)
1455	19.65	17.47	1446	60.29	1.25	1455	–	υPhII(55), υPhI(28)
1448	92.64	5.76	1437	53.98	5.48	–	–	$\delta_{as}CH_3$(91)
1441	18.86	5.32	1436	75.47	6.86	1432	1431	υPhII(55), υPhI(28)
1436	4.52	2.93	1420	8.84	1.86	–	–	υPhII(26), υPhI(48)
1434	6.21	3.27	1414	9.62	2.65	–	–	υPhII(15), υPhI(28), $\upsilon C_{26}N_5$(45)
		6.70	1382	41.51	2.56	1375	1378	$\delta_{s}CH_3$(91)
136937.52								
1309	10.99	10.93	1324	0.65	8.65	–	1321	υPhII(50), υPhI(36)
1299	22.80	1.12	1316	9.36	1.16	1315	1312	υPhII(42), υPhI(50)
1289	56.92	19.51	1284	43.49	19.83	–	1288	υCN(24), δCHI(13), $\upsilon_{as}SO_2$(43)
1268	86.05	7.44	1272	86.27	6.98	1278	–	δCHII(44), δCHI(34), δRngIII(12)
1250	182.96	7.31	1236	356/05	31.38	1245	1238	υCN(46), δCHII(12), δCHI(13)
1225	264.57	28.45	1217	8.83	23.93	1211	1209	υCN(55), δCHII(15), δCHI(23)
1217	8.95	18.28	1176	27.52	20.30	1172	1170	$\upsilon_{s}SO_2$(48), υCN(15), δCHII(11)
1177	42.57	25.88	1160	0.34	3.01	–	1157	δCHI(79)
1151	0.20	1.75	1160	1.97	8.97	–	1157	δCHII(74)
1150	0.85	12.17	1116	6.91	1.10	1122	1125	δCHI(19), δCHII(42), υPhI(16), υPhII(18)
1125	44.47	16.22	1107	0.06	1.85	1099	1106	δCHI(40), δCHII(12), υPhI(18), υPhII(11)
1120	5.27	3.68	1038	9.39	2.10	1054	1034	δCH_3(80)
1094	115.53	19.36	1026	12.03	2.41	1032	1021	δPhI(21), υPhI(52), δCHI(15)
1049	27.89	0.80	1023	16.99	1.83	–	1021	υPhII(44), δPhII(12), δCH_3(16)
1028	26.92	12.35	1007	1.24	46.03	1011	–	υPhI(16), δPhI(19), δCHI(55)
1025	2.95	5.78	1004	2.81	12.07	–	–	γCHI(52), γCHII(10)
1023	1.79	18.24	1003	1.02	2.00	–	–	γCHI(21), δCHII(67)
1018	27.45	25.76	1001	4.66	11.37	–	–	γCHII(64)

Table 1 (*continued*)

B3LYP/6-31G*			B3LYP/SDD			IR	Raman assignments	
υ	IR_I	R_A	υ	IR_I	R_A			
994	30.72	3.50	996	16.70	3.23	–	–	δCH_3(61), δPhII(15)
960	0.22	0.22	967	1.74	1.49	972	975	γCHI(58), γCHII(13)
957	0.26	0.15	965	1.20	0.73	963	–	γCHI(15), γCHII(67)
952	1.77	4.364	944	1.85	4.76	–	–	δPhI(27), υCC(41), δCN(12)
931	0.92	0.30	886	2.06	0.57	891	900	γCHI(68)
926	0.64	0.42	879	3.13	0.71	–	–	γCHII(69)
875	6.36	2.79	875	55.78	5.10	878	–	υCC(18), δPhII(31), γCHII(12), δPhI(11)
859	0.13	1.62	869	13.67	3.31	–	–	υCC(17), δPhII(41), γCHII(12)
851	0.18	2.30	778	88.24	0.40	768	777	γCHI(60), γCHII(19)
753	55.39	2.18	770	24.82	0.94	768	–	γCHI(27), γCHII(61)
747	8.99	3.92	760	107.55	5.38	768	754	τPhI(25), τPhII(19), τringIII(37)
733	4.65	3.13	733	6.30	5.60	740	726	τPhI(47), τPhII(15), τringIII(14)
719	41.72	1.76	717	0.23	1.01	721	–	τPhI(20), τPhIII(50)
714	3.94	0.62	696	1.81	0.70	–	–	δPhI(26), υCS(38), δPhII(20)
705	25.87	0.45	671	21.72	0.71	672	674	δPhII(24), δPhI(21), υCS(41)
656	0.99	15.19	642	2.61	19.33	638	638	δPhI(25), δPhII(36), δC=O(38)
626	7.08	0.78	623	6.13	0.63	612	610	δPhI(41), δPhII(26)
594	28.89	1.72	598	10.25	2.13	588	595	γC=O(35), γCN(24)
568	24.07	1.82	572	26.11	2.86	568	567	γC=O(12), τPhI(39)
561	36.63	0.74	531	12.70	3.07	530	540	τPhII(43), τringIII(12)
546	46.83	5.35	522	8.33	3.68	518	–	τPhII(43), τringIII(11), γC=O(14)
535	15.57	1.67	496	31.42	3.36	500	–	τPhI(15), δringIII(19), τCN(21)
500	10.42	0.54	475	27.35	1.33	473	475	τPhII(17), δC=O(13), δSO_2(31)
486	4.77	0.75	462	23.69	2.07	460	462	δSO_2(34), τPhI(22), δC=O(16)
448	9.82	2.26	443	0.58	2.89	–	–	τPhI(22), τCN(22), τPhII(34)
444	1.38	1.97	389	19.85	6.72	405	404	δC=O(19), τPhI(24)
397	9.88	4.63	386	21.60	8.99	–	–	δSO_2(32), τPhI(18), δRingIII(21)
384	8.23	2.36	374	4.32	4.30	–	–	δRingII(52), τPhII(16), δSO_2(12)
368	2.39	3.43	347	4.64	4.05	–	352	δC=O(19), τPhII(11), δSO_2(10)
342	1.19	7.26	328	2.80	8.47	–	327	τPhI(22), τPhII(13), δRingIII(10)
309	1.00	3.23	282	1.14	4.56	–	284	δRingII(19), δSO_2(38), τPhI(10)

(*continued on next page*)

Table 1 (*continued*)

B3LYP/6-31G*			B3LYP/SDD			IR	Raman assignments	
υ	IR_I	R_A	υ	IR_I	R_A			
304	4.39	0.92	280	6.05	1.58	–	284	τPhII(18), δCN(11), δSO_2(10), τCN(14)
271	1.66	0.45	246	4.96	5.17	–	228	δSO_2(35), τPhI(13), τPhII(17)
237	5.09	3.10	193	10.36	9.17	–	203	δSO_2(41), τPhII(16), δCN(17)
203	1.94	1.60	182	7.54	0.89	–	–	δSO_2(31), δCN(16)
190	0.34	1.59	176	1.67	3.18	–	168	δSO_2(39), τCS(12), τPhII(10)
152	1.86	5.04	136	0.79	6.19	–	139	δSO_2(39), τCS(35)
134	0.41	5.99	121	0.01	8.54	–	121	τRingIII(31), τCH_3(19), δSO_2(11)
114	0.15	6.63	103	1.42	2.11	–	99	τRingIII(32), τCH_3(24)
97	0.97	0.77	90	0.63	1.31	–	–	τRingIII(24), τCH_3(45)
74	0.15	7.54	75	0.37	7.31	–	–	τCS(46), τCH_3(15), τC=O(12)
65	4.12	0.87	64	6.10	1.18	–	–	τCH_3(14), τC=O(52)
49	4.12	3.92	47	5.78	3.28	–	–	τCH_3(31), τRingIII(22), τCN(15)

υ – Stretching; δ – in-plane deformation; γ – out-of-plane deformation; τ – twisting; the phenyl rings C_{16}—C_{17}—C_{19}—C_{21}—C_{23}—C_{25} and C_6—C_7—C_9—C_{11}—C_{13}—C_{15} are designated as PhI and PhII; RingIII-ring portion between PhI and PhII; as – asymmetric; s – symmetric; PED contribution is given in brackets in the assignment column.

1452, 1437 cm^{-1}. Experimentally the bands are observed at 1462 cm^{-1} in IR and at 1456 cm^{-1} in Raman spectrum. In many molecules the symmetric deformation $\delta_s CH_3$ appears with an intensity varying from medium to strong and expected in the range of 1380 ± 25 cm^{-1} [53]. Bands at 1375 cm^{-1} in the IR spectrum, 1378 cm^{-1} in the Raman spectrum and at 1382 cm^{-1} (SDD) are assigned as $\delta_s CH_3$ modes for the title compound. Esters display a methyl rock in the neighborhood of 1045 cm^{-1} [53]. The second rock in the region 970 ± 70 cm^{-1} [53] is more difficult to find among the C—H out-of-plane deformations. For the title compound, these modes ρCH_3 are calculated at 1038 and 996 cm^{-1}. The bands at 1054 cm^{-1} in the IR and at 1034 cm^{-1} in the Raman spectrum are assigned as ρCH_3 modes.

Primary aromatics with nitrogen directly on the ring absorb at 1330–1200 cm^{-1} because of the stretching of the phenyl C—N bond [57]. For the title compound, the υC_{16}—N_5 and υC_{15}—N_5 modes are observed at 1245, 1211 cm^{-1} in the IR spectrum, 1238, 1209 cm^{-1} in the Raman spectrum and at 1236, 1217 cm^{-1} theoretically (SDD). Panicker et al. [58] reported the CN stretching modes at 1219, 1237 (IR) and at 1292, 1234, 1200 cm^{-1} theoretically. The C_{26}—N_5 stretching vibration is only weakly to moderately active in the region 1400 ± 70 cm^{-1}, when the nitrogen atom is bound to a carbonyl group [53] and in the present case, the SDD calculation give this mode at 1414 cm^{-1}.

The asymmetric and symmetric stretching modes of SO_2 group appear in the region 1315 ± 45 and 1150 ± 30 cm^{-1} [53]. The observed bands at 1172 cm^{-1} in the IR spectrum, 1288, 1170 in the Raman spectrum and at 1284, 1176 cm^{-1} theoretically (SDD) are assigned as SO_2 stretching modes. The modes are not pure, but contain significant contributions from other modes also. Although the region of SO_2 scissors (540 ± 60 cm^{-1}) and that of SO_2 wagging (500 ± 55 cm^{-1}) partly overlap, the two vibrations appear separately [53]. These deformation bands of SO_2 are assigned at 473, 460 cm^{-1} in the IR spectrum, 475, 462 cm^{-1} in the Raman spectrum and at 475, 462 cm^{-1} theoretically. Chohan et al. [59] reported the SO_2 stretching vibrations at 1345, 1110 cm^{-1}. Hangen et al. [60] reported SO_2 modes at 1314, 1308, 1274, 1157, 1147, 1133 cm^{-1} for sulfonamide derivatives. The twisting and rocking modes of SO_2 are expected at 420 ± 75 and 345 ± 55 cm^{-1} [53]. The bands observed at 386 and 282 cm^{-1} theoretically are assigned as the twisting and rocking modes of SO_2. Varghese et al. reported $\upsilon_{as} SO_2$ at 1313 cm^{-1} in IR and at 1315 cm^{-1} in Raman spectra and the symmetric $\upsilon_s SO_2$ at 1147 cm^{-1} in IR and at 1157 and 1136 cm^{-1} in Raman spectrum [61]. For the title compound, the C—S stretching vibration [53] appears at 672 cm^{-1} in the IR spectrum, 674 cm^{-1} in the Raman spectrum and the theoretically calculated values (SDD) are 696 and 671 cm^{-1}. The C—S stretching mode is reported at about 640 cm^{-1} for dithienothiophenes by Cravino et al. [62].

The existence of one or more aromatic ring in the structure is normally determined from the C—H and C—C ring related vibrations. The C—H stretching occurs above 3000 cm^{-1} and is typically exhibited as multiplicity of weak to moderate bands, compared with the aliphatic C—H stretching [63]. In the present case, the SDD calculations give υC—H modes of the phenyl rings in the range 3085–3147 cm^{-1}. The bands observed at 3095 cm^{-1} in the IR spectrum and at 3091 cm^{-1} in the Raman spectrum are assigned to the υC—H modes of the phenyl ring. The benzene ring possesses six ring-stretching vibrations, of which the four with the highest wavenumbers (occurring near 1600, 1580, 1490 and 1440 cm^{-1}) are good group vibrations [53]. With heavy substituents, the band tends to shift to somewhat lower wavenumbers. In the absence of ring conjugation, the band at 1580 cm^{-1} is usually weaker than that at 1600 cm^{-1}. In the case of C=O substitution, the band near

1490 cm^{-1} can be very weak. The fifth ring-stretching vibration is active near 1315 ± 65 cm^{-1}, a region that overlaps strongly with that of the CH in-plane deformation. The sixth ring-stretching vibration or the ring breathing mode appears as a weak band near 1000 cm^{-1} in mono, 1,3-di and 1,3,5-trisubstituted benzenes [53,64]. In the otherwise substituted benzenes, however, this vibration is substituent sensitive and difficult to distinguish from the ring in-plane deformation [53,64]. In the following discussion the phenyl rings C_{16}—C_{17}—C_{19}—C_{21}—C_{23}—C_{25} and C_6—C_7—C_9—C_{11}—C_{13}—C_{15} are designated as PhI and PhII. The υPh modes are expected in the region 1260–1615 cm^{-1} for the ortho substituted phenyl rings. The υPh modes are observed at 1581, 1455, 1432, 1315, 1032 cm^{-1} in the IR spectrum, at 1584, 1431, 1321, 1312, 1021 cm^{-1} in the Raman spectrum and theoretically (SDD) at 1573, 1559, 1446, 1420, 1316, 1026 for the phenyl ring PhI and at 1585, 1550, 1446, 1436, 1324, 1023 for the phenyl ring PhII. In ortho di-substitution the ring breathing mode has three frequency intervals according to whether both substituents are heavy, or one of them is heavy while the other is light, or both of them are light. In the first case, the interval is 1100–1130 cm^{-1}, in the second case 1020–1070 cm^{-1}, while in the third case it is between 630 and 780 cm^{-1} [64]. The SDD calculations give bands at 1026 and 1023 cm^{-1} as the ring breathing modes in the present case.

The C—H out-of-plane deformations of the phenyl ring [53] are observed in the range 1000–700 cm^{-1}. Generally, the C—H out-of-plane deformations with the highest wavenumber have weaker intensity than those absorbing at lower wavenumber. The out-of-plane CH vibrations are observed at 972, 891, 768 cm^{-1} in the IR spectrum, at 975, 900, 777 cm^{-1} in the Raman spectrum, at 1004, 967, 886, 778 cm^{-1} theoretically for PhI and at 963, 768 cm^{-1} in the IR spectrum, at 1001, 965, 879, 770 cm^{-1} theoretically (SDD) for PhII. The strong CH occurring at 755 ± 35 cm^{-1} is typical for 1,2-disubstitution and the band observed at 768 cm^{-1} in the IR spectrum is assigned to this mode, which finds support from computational results. The CH in-plane deformation bands of the benzene ring are expected above 1000 cm^{-1} [53] and in the present case, the bands observed at 1278, 1099, 1011 cm^{-1} in the IR spectrum, 1157, 1106 cm^{-1} in the Raman spectrum, 1272, 1160, 1107, 1007 cm^{-1} theoretically and 1278, 1122 cm^{-1} in the IR spectrum, 1157, 1125 cm^{-1} in the Raman spectrum, 1272, 1160, 1116, 1003 cm^{-1} theoretically are assigned as the in-plane CH deformation modes of the phenyl rings PhI and PhII, respectively.

The substituent sensitive modes of the phenyl ring are also identified and assigned.

Geometrical parameters and first hyperpolarizability

For the title compound, the C=O bond length is 1.2482 (XRD) and 1.2102 Å (SDD). Dandia et al. [65] reported this bond length as 1.343 Å and Jadeja et al. [66] reported this as 1.252 Å. Lasibal et al. [67] reported the bond lengths SO = 1.4269–1.4129, SC = 1.7582 Å whereas the corresponding values for the title compound are SO = 1.4813, 1.4810 (SDD), 1.4294, 1.4292 (XRD), SC = 1.8641, 1.8608 (SDD), 1.7557, 1.7524 Å (XRD). The values of bond angles O_2—S_1—O_3 = 118.6, O_2—S_1—C_{25} = 108.9, O_3—S_1—C_{25} = 104.9, $O_{2,3}$—S_1—C_6 = 107.9–108.3° reported by Lasibal et al. [67] are in agreement with the corresponding values, 119.6, 117.7 (SDD and XRD), 108.7, 108.4 (SDD and XRD), 109.5, 110.2 (SDD and XRD), 110.1–109.9, 109.2–110.0° (SDD and XRD) of the title compound.

For the title compound, the C—N bond lengths C_{15}—N_5 = 1.4473 (SDD), 1.4314 (XRD) and C_{16}—N_5 = 1.4412 (SDD), 1.4283 Å (XRD). Dandia et al. [65] reported corresponding bond lengths for C—N as 1.364 and 1.412 Å for similar derivative and Endredi et al. [68] reported these values as 1.408 and 1.412 Å, Jadeja et al. [66] reported this as 1.428 Å and Tamasi et al. [69] reported this as 1.378, 1.377 and 1.397 Å. The SDD calculations give the bond length C_{26}—N_5 as 1.4240, whereas the corresponding XRD value is 1.3942 Å. The C—H of the CH_3 at C_{27} are C_{27}—H_{28} = 1.0927 (SDD), 0.98 (XRD); C_{27}—H_{29} = 1.0933 (SDD), 0.98 (XRD); C_{27}—H_{30} = 1.0965 (SDD), 0.98 Å (XRD).

The C_6—S_1—C_{25} bond angle of the title compound is 96.5° (99.9°). Dandia et al. [65] reported as 101.3° and Endredi et al. [68] reported this value as 96.1°, 97.9°, and 98.0°. The C_{15}—N_5—C_{26}, C_{16}—N_5—C_{26} and C_{16}—N_5—C_{15} bond angle of the title compound for SDD and XRD are 119.8 (118.5), 122.6 (123.6) and 117.5 (116.5°). The asymmetry of the bond angle values is due to the interaction of N—C=O with hydrogen atoms of CH_3 moiety. Dandia et al. [65] reported these values as 119.0° 114.0° and 126.6°. The bond angles of the compound are C_{17}—C_{16}—C_{25} = 117.4 (SDD), 118.5 (XRD); C_{17}—C_{16}—N_5 = 121.9 (SDD), 122.8 (XRD); C_{16}—C_{25}—C_{23} = 123.7 (SDD), 121.9 (XRD); C_{16}—C_{25}—S_1 = 116.2 (SDD), 117.4° (XRD). Dandia et al. [65] reported these values as 122.1°, 124.9°, and 113.0°. The three bond angles around C_{25} given by SDD are 116.2°, 120.1°, 123.7° and by XRD are 117.4°, 120.8°, 121.9°. The bond angle value 116.2° reveals the reduction of C_{16}—C_{25}—S_1 is due to the slight interaction of the lone pairs of sulfur with H_{24} and H_8 of aromatic rings [68].

The torsion angles of the compound are C_{19}—C_{17}—C_{16}—N_5 = 176.7 (SDD), 179.5 (XRD); C_{17}—C_{16}—N_5—C_{15} = −129.4 (SDD), −132.0 (XRD); C_{21}—C_{23}—C_{25}—S_1 = 178.7 (SDD), 177.9 (XRD); C_{23}—C_{25}—S_1—C_6 = 138.0 (SDD), 142.4 (XRD); C_{11}—C_{13}—C_{15}—N_5 = −177.7 (SDD), −178.9 (XRD); C_{13}—C_{15}—N_5—C_{16} = 132.6 (SDD), 133.6 (XRD); C_9—C_7—C_6—S_1 = −177.3 (SDD), −178.8 (XRD); C_7—C_6—S_1—C_{25} = −139.0 (SDD), −140.6° (XRD). The thiazine moiety is slightly folded along the N—S axis which is evident from the torsion angle values N_5—C_{15}—C_6—C_7 = 177.2 (XRD), 176.3 (SDD), S_1—C_{25}—C_{16}—C_{17} = 178.7 (XRD), 179.9 (SDD), S_1—C_{25}—C_{16}—N_5 = −2.3 (XRD), −4.6 (SDD), and C_{17}—C_{16}—N_5—C_{15} = −132.0 (XRD), −129.4° (SDD).

Nonlinear optical (NLO) effects arise from the interactions of electromagnetic fields in various media to produce new fields altered in phase, frequency, amplitude or other propagation characteristic from the incident fields. The first order hyperpolarizabilty (β) of the title molecule is calculated using B3LYP/SDD method. First order hyperpolarizability is a third rank tensor that can be described by 3 × 3 × 3 matrices. The 27 components of the 3D matrix can be reduced to 10 components due to the Kleinman symmetry [70]. It can be given in the lower tetrahedral format. It is obvious that the lower part of the 3 × 3 × 3 matrices is a tetrahedral. The components of β are defined as the coefficients in the Taylor series expansion of the energy in the external electric field. When the external electric field is weak and homogenous, this expansion becomes:

$$E = E_0 - \sum_i \mu_i F^i - \frac{1}{2}\sum_{ij} \alpha_{ij} F^i F^j - \frac{1}{6}\sum_{ijk} \beta_{ijk} F^i F^j F^k - \frac{1}{24}\sum_{ijkl} \gamma_{ijkl} F^i F^j F^k F^l + \cdots$$

where E_0 is the energy of the unperturbed molecule, F^i is the field at the origin, μ_{ij}, α_{ij}, β_{ijk} and γ_{ijkl} are the components of dipole moment, polarizability, the first hyperpolarizabilities, and second hyperpolarizibilities, respectively. The calculated first hyper polarizability of the title compound is 2.33 × 10^{-30} esu and which is 17.92 times that of the standard NLO material urea (0.13 × 10^{-30} esu) [71]. We conclude that the title compound is an attractive object for future studies of nonlinear optical properties.

Molecular electrostatic potential analysis

Electrostatic potential maps, also known as electrostatic potential energy maps, or molecular electric potential surface, illustrate

the charge distributions of molecules three dimensionally. The purpose of finding the electrostatic potential is to find the reactive site of a molecule. These maps allow us to visualize variably charged regions of a molecule. Knowledge of the charge distributions can be used to determine how molecules interact with one another. Molecular electrostatic potential (MEP) mapping is very useful in the investigation of the molecular structure with its physiochemical property relationships [72–74]. Total SCF electron density surface mapped with the molecular electrostatic potential of the title compound is shown in Fig. 6. The molecular electrostatic potential surface which is a 3D plot of electrostatic potential mapped onto the iso-electron density surface simultaneously displays molecular shape, size and electrostatic potential values. The color scheme for the MEP surface is red-electron rich or partially electron negative; blue-electron deficient or partially positive charge; light blue-slightly electron deficient region; yellow-slightly electron rich region, respectively. Areas of low potential, red are characterized by an abundance of electrons. Areas of high potential, blue are characterized by a relative absence of electrons. The different values of the electrostatic potential at the surface are represented by different colors. Potential increases in the order red < orange < yellow < green < blue. Blue indicates strongest attraction and red indicates the strongest repulsion. The negative (red and yellow) regions of MEP were related to electrophilic reactivity and the positive (blue) regions to nucleophilic reactivity. Oxygen has a higher electro negativity value would consequently have a higher electron density around them. Thus the spherical region that corresponds to nitrogen atom would have a red portion on it. The MEP of the title compound clearly indicates the electron rich centers of nitrogen, oxygen atoms. The MEP map shows that the negative potential sites are on electronegative atoms as well as the positive potential site are around the nitrogen atoms. These sites give information about the region from where the compound can have non covalent interactions. According to these calculated results, the MEP shows that the negative potential sites are on oxygen atoms and the positive potential sites are around the nitrogen atoms. These sites give information about the region from where the compound can have intermolecular interactions.

Frontier molecular orbital analysis

The most widely used theory by chemists is the molecular orbital (MO) theory. It is important that ionization potential I, electron affinity A, electrophilicity index ω, chemical potential μ, electronegativity χ, hardness η and softness S be put into a MO framework. Based on density functional descriptors global chemical reactivity descriptors of compounds such as hardness, chemical potential, softness, electro negativity and electrophilicity index as well as local reactivity has been defined [75–77]. Pauling introduced the concept of electronegativity as the power of an atom in a compound to attract electrons to it. Using Koopman's theorem for closed shell components η, μ and χ can be defined as $\eta = I - A$; $\mu = (I - A)/2$; $\chi = (I + A)/2$; where I and A are the ionization potential and electron affinity of the compounds respectively. The ionization energy and electron affinity can be expressed through HOMO and LUMO orbital energies as $I = -E_{HOMO}$ and $A = -E_{LUMO}$. Electron affinity refers to the capability of ligand to accept precisely one electron from a donor. However in many kinds of bonding viz. covalent hydrogen bonding, partial charge transfer takes place. The ionization potential given by SDD method for the title compound is 9.112 eV. Considering the chemical hardness, large HOMO–LUMO gap means a hard molecule and small HOMO–LUMO gap means a soft molecule. One can also relate the stability of the molecule to hardness, which means that the molecule with least HOMO–LUMO gap means, it is more reactive. Parr et al. [75] have defined a new descriptor to quantity the global electrophilic power of the compound as electrophilicity index (ω) which defines a quantitative classification of global electrophilic nature of a compound. Parr et al. have proposed electrophilicity index (ω) as a measure of energy lowering due to maximal electron flow between donor and acceptor. They defined electrophilicity index as follows: $\omega = \mu^2/2\eta$. The usefulness of this new reactivity quantity has been recently demonstrated understanding the toxicity of various pollutants in terms of their reactivity and site selectivity [78]. The calculated vales of hardness, softness and electrophilicity index are 3.7808, 0.132 and 7.2216. The calculated value of electrophilicity index describes the biological activity of the title compound. The atomic orbital components of the frontier molecular orbital are shown in Fig. 7.

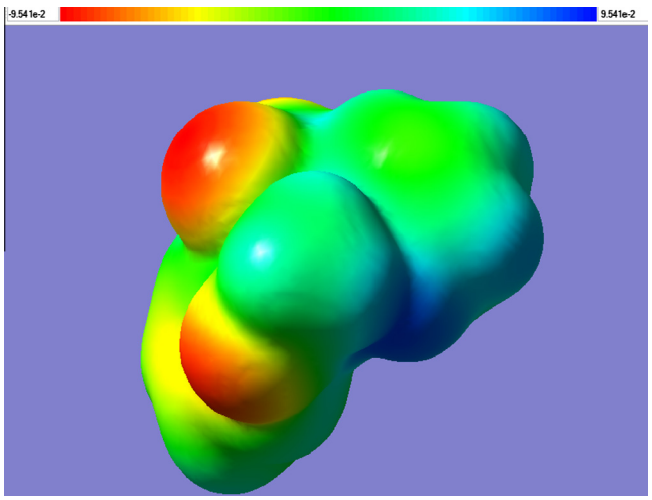

Fig. 6. MEP of 1-(5,5-dioxido-10H-phenothiazin-10-yl)ethanone.

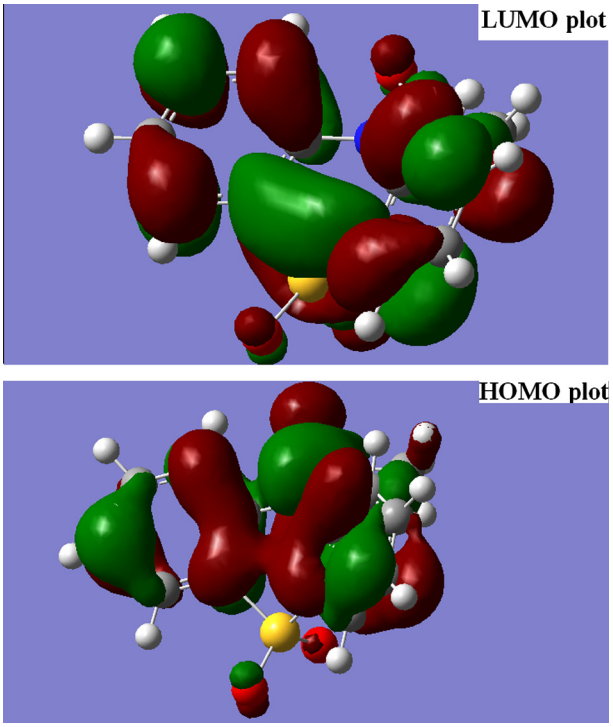

Fig. 7. HOMO and LUMO plots of 1-(5,5-dioxido-10H-phenothiazin-10-yl)ethanone.

NBO analysis

The natural bond orbital (NBO) calculations were performed using NBO 3.1 program as implemented in the Gaussian 09 package at the DFT/B3LYP level in order to understand various second-order interactions between the filled orbital of one subsystem and vacant orbital of another subsystem, which is a measure of the intermolecular delocalization or hyper conjugation. NBO analysis provides the most accurate possible 'natural Lewis structure' picture of 'j' because all orbital details are mathematically chosen to include the highest possible percentage of the electron density. A useful aspect of the NBO method is that it gives information about interactions of both filled and virtual orbital spaces that could enhance the analysis of intra and inter molecular interactions.

The second-order Fock-matrix was carried out to evaluate the donor–acceptor interactions in the NBO basis. The interactions result in a loss of occupancy from the localized NBO of the idealized Lewis structure into an empty non-Lewis orbital. For each donor (i) and acceptor (j) the stabilization energy ($E(2)$) associated with the delocalization $i \rightarrow j$ is determined as

$$E(2) = \Delta E_{ij} = q_i \frac{(F_{i,j})^2}{(E_j - E_i)}$$

where q_i is the donor orbital occupancy, E_i, E_j is diagonal elements and F_{ij} is the off diagonal NBO Fock matrix elementIn NBO analysis large $E(2)$ value shows the intensive interaction between electron-donors and electron-acceptors and greater the extent of conjugation of the whole system, the possible intensive interactions are given in Table 2. The second-order perturbation theory analysis of Fock matrix in NBO basis shows strong intra-molecular hyper-conjugative interactions of π electrons. The intra-molecular hyper-conjugative interactions are formed by the orbital overlap between n(O) and σ*(S—O) bond, orbital which results in ICT causing stabilization of the system. The strong intra-molecular hyper-conjugative interaction of S_1—O_3 from of $n3(O_2) \rightarrow \sigma^*(S_1—O_3)$ which increases ED (0.13355e) that weakens the respective bonds leading to stabilization of 19.70 kcal mol^{-1}. Also another intra-molecular hyper-conjugative interactions are formed by the orbital overlap between n(O) and σ*(S—C) bond orbital which results in ICT causing stabilization of the system. The strong intra-molecular hyper-conjugative interaction of S_1—C_{25} from of $n3(O_3) \rightarrow \sigma^*(S_1—C_{25})$ which increases ED(0.20884e) that weakens the respective bonds leading to stabilization of 13.58 kcal mol^{-1}. Another hyper-conjugative interaction of O_4—C_{26} from of $n3(O_4) \rightarrow \pi^*(O_4—C_{26})$ which increases ED(0.2225e) that weakens the respective bonds leading to stabilization of 38.32 kcal mol^{-1}. These interactions are observed as an increase in electron density (ED) in C—C anti-bonding orbital that weakens the respective bonds.

The increased electron density at the oxygen, atoms leads to the elongation of respective bond length and a lowering of the corresponding stretching wavenumber. The electron density (ED) is transferred from the n(O), to the anti-bonding σ*, π* orbital of the S—O, S—C, O—C explaining both the elongation and the red shift. The —C═O, N—C stretching modes can be used as a good probe for evaluating the bonding configuration around the corresponding atoms and the electronic distribution of the molecule. Hence the above structure is stabilized by these orbital interactions [79].

The NBO analysis also describes the bonding in terms of the natural hybrid orbital $n3(O_2)$, which occupy a higher energy orbital (−0.27119 a.u) with considerable p-character (99.90%) and low occupation number (1.84286 a.u) and the other $n2(O_2)$ occupy a lower energy orbital (−0.27205) with p-character (100.0%) and high occupation number (1.86731 a.u). Also $n3(O_3)$, which occupy a higher energy orbital (−0.28053 a.u) with considerable p-character (99.98%) and low occupation number (1.85983 a.u) and the other $n2(O_3)$ occupy a lower energy orbital (−0.28090 a.u) with p-character (99.75%) and high occupation number (1.86712 a.u). Also $n3(O_4)$, which occupy a higher energy orbital (−0.27427 a.u) with considerable p-character (99.95%) and low occupation number (1.69458 a.u) and the other $n2(O_4)$ occupy a lower energy orbital (−0.29499 a.u) with p-character (99.99%) and high occupation number (1.87752 a.u). Thus, a very close to pure p-type lone pair orbital participates in the electron donation to the σ*(S—O) orbital for $n3(O_2) \rightarrow \sigma^*(S_1—O_3)$, $\sigma^*(S_1—C_{25})$ orbital for $n3(O_3) \rightarrow \sigma^*(S—C)$ and π^*(O—C) orbital for $n3(O_4) \rightarrow \pi^*(O_4—C_{26})$ interactions in the compound. The results are given as supporting information in Table S2.

Conclusion

FT-IR and FT-Raman spectra of 1-(5,5-dioxido-10H-phenothiazin-10-yl)ethanone were recorded and analyzed experimentally

Table 2
Second order perturbation theory analysis of Fock matrix in NBO basis corresponding to the intra-molecular bonds of the title compound.

Donor (i)	Type	ED/e	Acceptor (j)	Type	ED/e	$E(2)$[a]	$E(j) - E(i)$[b]	$F(i, j)$[c]
S1—O2	σ	1.97051	S1—O3	σ*	0.13355	3.76	0.82	0.051
S1—O3	σ	1.97753	S1—O2	σ*	0.14114	3.90	0.84	0.053
C2—C3	σ	1.96007	C13—C15	σ*	0.02732	4.23	1.20	0.064
S1—C25	σ	1.96063	C16—C17	π*	0.02872	4.55	1.18	0.066
C6—C7	π	1.69766	C13—C15	π*	0.34905	22.03	0.30	0.073
C7—C9	σ	1.97094	S1—C6	σ*	0.20669	6.20	0.76	0.064
C9—C11	π	1.64197	C6—C7	π*	0.38041	25.26	0.27	0.074
C13—C15	σ	1.96510	S1—C6	σ*	0.20669	5.76	0.77	0.062
C13—C15	π	1.63828	C6—C7	π*	0.38041	22.02	0.28	0.070
C16—C17	π	1.65057	C1—C6	π*	0.36678	21.05	0.29	0.070
C23—C25	π	1.68629	C16—C17	π*	0.36943	23.26	0.29	0.074
LP(1)O2	σ	1.97878	S1—O3	σ*	0.13355	1.27	0.95	0.032
LP(2)O2	n	1.86731	S1—C6	σ*	0.20669	10.17	0.32	0.052
LP(3)O2	n	1.84286	S1—O3	σ*	0.13355	19.70	0.31	0.070
LP(1)O3	n	1.98096	S1—O2	σ*	0.14114	1.11	0.95	0.030
LP(2)O3	n	1.86712	S1—O2	σ*	0.14114	17.64	0.33	0.068
LP(3)O3	n	1.85983	S1—C25	σ*	0.20884	13.58	0.32	0.060
LP(1)O4	n	1.97372	C26—C27	σ*	0.04598	2.60	1.03	0.046
LP(2)O4	n	1.87752	N5—C26	σ*	0.09868	26.43	0.60	0.113
LP(3)O4	n	1.69458	O4—C26	π*	0.22250	38.32	0.28	0.095

[a] $E(2)$ means energy of hyper-conjugative interactions (stabilization energy in kcal/mol.).
[b] Energy difference (a.u.) between donor and acceptor i and j NBO orbitals.
[c] $F(i, j)$ is the Fock matrix elements (a.u.) between i and j NBO orbitals.

and theoretically. Potential energy distribution of normal modes of vibrations was done using GAR2PED program. The HOMO and LUMO analysis is used to determine the charge transfer within the molecule. The calculated vales of hardness, softness and electrophilicity index are 3.7808, 0.132 and 7.2216. The calculated value of electrophilicity index describes the biological activity of the title compound. The stability of the molecule arising from hyper conjugative interaction and charge delocalization has been analyzed using NBO analysis. Molecular electrostatic potential was performed by the DFT method and infrared intensities and Raman activities are also reported. MEP shows that the negative potential sites are on oxygen atoms and the positive potential sites are around the nitrogen atoms. The geometrical parameters of the title compound (SDD) are in agreement with XRD crystal structure data. The calculated first hyperpolarizability of the title compound is 2.33×10^{-30} esu and which is 17.92 times that of the standard NLO material urea and is an attractive object for future studies of nonlinear optics.

Acknowledgements

M.K. is grateful to CPEPA, UGC for the award of a JRF and the authors are thankful to University of Antwerp for access to the university's CalcUA Supercomputer Cluster.

Appendix A. Supplementary material

Supplementary data associated with this article can be found, in the online version, at http://dx.doi.org/10.1016/j.saa.2013.10.032.

References

[1] M.T. Miller, P.K. Gantzel, T.B. Karpishin, J. Am. Chem. Soc. 121 (1999) 4292–4293.
[2] C.G. Wemuth, The Practice of Medicinal Chemistry, second ed., Academic Press, London, 2003.
[3] J. Wang, M. Dong, J. liang, Z. Chang, S. Feng, H. Wang, N. Ding, Clin. J. Lab. Diag. 12 (2008) 381–382.
[4] M. Lam, N.L. Oleinick, A.L. Nieminen, J. Biol. Chem. 276 (2001) 47379–47386.
[5] S.H. Snyder, Am. J. Psych. 133 (1976) 197–202.
[6] O. Bartfos, J.O. Haug, Acta Psych. Scand. 60 (1979) 1–9.
[7] C. Bodea, I.A. Silberg, in: A.R. Katrizky, A.J. Boulton (Eds.), Advances in Heterocyclic Chemistry, Academic Press, New York, 1968.
[8] B. Keshavan, J. Seetharamappa, Polyhedron 6 (1987) 465–471.
[9] R.R. Gupta, Bioactive molecules: phenothiazine and 1,4-benzothiazines, Chemical and Biological Aspects, vol. 4, Elsevier, Amsterdam, 1988.
[10] M.L. Laws, R.R. Roberts, J.M. Nicholson, R. Butcher, J.P. Stables, A.M. Goodwin, C.A. Smith, K.R. Scott, Bioinorg. Med. Chem. 6 (1998) 2289–2299.
[11] H. Kai, Y. Morioka, Y. Koriyama, K. Okamoto, Y. Hasegawa, M. Hattori, K. Koika, H. Chiba, S. Shinohara, Y. Iwamoto, K. Takahashi, N. Tanimoto, Bioorg. Med. Chem. Lett. 18 (2008) 6444–6447.
[12] R.J. Baldessarini, F.I. Tarazi, in: J.G. Hardman, L.E. Limbird, A.G. Gilman (Eds.), Goodman and Gilman's the Pharmacological Basis of Therapeutics, 10th ed., McGraw Hill Companies Inc., New York, 2001.
[13] G. Chouinard, L. Annable, A.R. Chouinard, M.L. Kropsky, J. Clin. Psych. 40 (1979) 147–152.
[14] G. Gardos, I. Samu, M. Kallos, J.O. Cole, Psycho-Pharmacol. 71 (1980) 29–34.
[15] H.S. Gowda, J.B. Raj, J. Indian Chem. Soc. 59 (1982) 1398–1402.
[16] J. Karpinska, A. Kojlo, W. Misiuk, B. Starczewska, H.P. Tarasiewicz, J. Trace Microprobe Technol. 18 (2000) 369–379.
[17] F. Fukasawa, J. Karpinska, H.P. Tarasiewicz, J. Trace Microprobe Technol. 13 (1995) 421–429.
[18] E. Bacu, G.C. Chitanu, A. Couture, P. Grandclaudon, G.H. Singurel, A. Carpov, Eur. Polym. J. 38 (2002) 1509–1513.
[19] S. Darvesh, R. McDonald, A. Penwell, S. Conrad, K.V. Darvesh, D. Mataija, G. Gomez, A. Caines, R. Walsh, E. Martin, Bioorg. Med. Chem. 13 (2005) 211–222.
[20] A. Saxena, A.M. Redman, X. Jiang, O. Lockridge, B.P. Doctor, Biochemistry 36 (1997) 14642–14651.
[21] J. Debord, L. Merle, J.C. Bollinger, T. Dantoine, J. Enzym. Inhib. Med. Chem. 17 (2002) 197–202.
[22] B. Keshavan, J. Seetharamappa, Synth. React. Met. Org. Chem. 16 (1986) 979–989.
[23] B. Keshavan, R. Janardhan, Indian J. Chem. 26A (1987) 975–978.
[24] B. Keshavan, R. Janardhan, Indian J. Chem. 25A (1986) 1054–1056.
[25] H.S. Gowda, M. Jayarama, J. Inorg. Nucl. Chem. 43 (1981) 2329–2333.
[26] R. Kroener, M.J. Heeg, E. Deutsch, Inorg. Chem. 27 (1988) 558–566.
[27] N.M.M. Gowda, H.P. Phyu, Trans. Metal Chem. 17 (1992) 467–470.
[28] N.M.M. Gowda, H.P. Phyu, B.E. Ackerson, Trans. Metal Chem. 18 (1993) 64–68.
[29] N.M.M. Gowda, H.L. Pacquette, D.H. Kim, B. Jayaram, J. Mol. Struct. 382 (1996) 129–135.
[30] H.S. Gowda, S.A. Ahmed, J. Indian Chem. Soc. 55 (1978) 352–356.
[31] N.M.M. Gowda, R.K. Vallabhaneni, I. Gajula, S. Ananda, J. Mol. Struct. 407 (1997) 125–130.
[32] H. Puzanowska-Tarasiewicz, L. Kuzmicka, W. Misiuk, E. Regulska, Anal. Lett. 41 (2008) 2893–2911.
[33] M. Jayarama, V. D'Souza, H.S. Yathirajan, Talanta 33 (1998) 352–354.
[34] B.N. Achar, M.A. Ashok, Mater. Chem. Phys. 108 (2008) 8–15.
[35] M. Sailer, A.W. Franz, T.J.J. Muller, Chem. Eur. J. 14 (2008) 2602–2614.
[36] M. Sailor, M. Nonnenmacher, T. Oeser, T.J.J. Muller, Eur. J. Org. Chem. 2 (2006) 423–435.
[37] G.W. Kim, M.J. Cho, Y.J. Yu, Z.H. Kim, J.K. Jin, D.Y. Kim, D.H. Choi, Chem. Mater. 19 (2007) 42–50.
[38] N.S. Cho, J.H. Park, S.K. Lee, J. Lee, H.K. Shim, M.J. Park, D.H. Huang, B.J. Jung, Macromolecules 39 (2006) 177–183.
[39] C.O. Okafor, Dyes Pig. 7 (1986) 249–287.
[40] M. Hauck, J. Schonhaber, A.J. Zucchero, K.I. Hardcastle, T.J.J. Muller, U.H.F. Bunz, J. Org. Chem. 72 (2007) 6714–6725.
[41] C.L. Honeybourne, R.J. Ewen, K.J. Alkins, in: R.A. Hann, D. Bloor (Eds.), Inorganic Materials for Non-linear Optics, Royal Society of Chemistry, Burlington House, London, 1989.
[42] W.Y. Wong, W.C. Chow, K.Y. Cheung, M.K. Fung, A.B. Djurisic, W.K. Chan, J. Organomet. Chem. 694 (2009) 2717–2726.
[43] W.T.A. Harrision, M.A. Ashok, H.S. Yathirajan, B.N. Achar, Acta Cryst. E63 (2007) o3277–o3278.
[44] J.P. Jasinski, A.E. Pek, P.S. Nayak, B. Narayana, H.S. Yathirajan, Acta Cryst. E 67 (2011) o430–o431.
[45] M.S. Siddegowda, J.P. Jasinski, James A. Golen, H.S. Yathirajan, Acta Cryst. E 67 (2011) o1702–o1703.
[46] M.J. Frisch, G.W. Trucks, H.B. Schlegel, G.E. Scuseria, M.A. Robb, J.R. Cheeseman, G. Scalmani, V. Barone, B. Mennucci, G.A. Petersson, H. Nakatsuji, M. Caricato, X. Li, H.P. Hratchian, A.F. Izmaylov, J. Bloino, G. Zheng, J.L. Sonnenberg, M. Hada, M. Ehara, K. Toyota, R. Fukuda, J. Hasegawa, M. Ishida, T. Nakajima, Y. Honda, O. Kitao, H. Nakai, T. Vreven, J.A. Montgomery Jr., J.E. Peralta, F. Ogliaro, M. Bearpark, J.J. Heyd, E. Brothers, K.N. Kudin, V.N. Staroverov, T. Keith, R. Kobayashi, J. Normand, K. Raghavachari, A. Rendell, J.C. Burant, S.S. Iyengar, J. Tomasi, M. Cossi, N. Rega, J.M. Millam, M. Klene, J.E. Knox, J.B. Cross, V. Bakken, C. Adamo, J. Jaramillo, R. Gomperts, R.E. Stratmann, O. Yazyev, A.J. Austin, R. Cammi, C. Pomelli, J.W. Ochterski, R.L. Martin, K. Morokuma, V.G. Zakrzewski, G.A. Voth, P. Salvador, J.J. Dannenberg, S. Dapprich, A.D. Daniels, O. Farkas, J.B. Foresman, J.V. Ortiz, J. Cioslowski, D.J. Fox, Gaussian 09, Revision B.01, Gaussian Inc., Wallingford, CT, 2010.
[47] J.B. Foresman, in: E. Frisch (Ed.), Exploring Chemistry with Electronic Structure Methods: A Guide to Using Gaussian, Gaussian Inc., Pittsburg, PA, 1996.
[48] P.J. Hay, W.R. Wadt, J. Chem. Phys. 82 (1985) 270–283.
[49] J.Y. Zhao, Y. Zhang, L.G. Zhu, J. Mol. Struct. Theochem. 671 (2004) 179–187.
[50] R. Dennington, T. Keith, J. Millam, GaussView, Version 5, Semichem Inc., Shawnee Mission KS, 2009.
[51] E.D. Glendening, A.E. Reed, J.E. Carpenter, F. Weinhold, NBO Version 3.1.
[52] J.M.L. Martin, C. Van Alsenoy, GAR2PED, A Program to Obtain a Potential Energy Distribution from a Gaussian Archive Record, University of Antwerp, Belgium, 2007.
[53] N.P.G. Roeges, A Guide to the Complete Interpretation of Infrared Spectra of Organic Structures, Wiley, New York, 1994.
[54] M. Barthes, G. De Nunzio, M. Ribet, Synth. Met. 76 (1996) 337–340.
[55] C.Y. Panicker, H.T. Varghese, D. Philip, H.I.S. Nogueira, K. Kastkova, Spectrochim. Acta A 67 (2007) 1313–1320.
[56] A. Bieliauskas, V. Martynaitis, V. Getautis, T. Malinauskas, V. Jankauskas, E. Kamarauskas, W. Holzer, A. Sackus, Tetrahedron 68 (2012) 3552–3559.
[57] N.B. Colthup, L.H. Daly, S.E. Wiberly, Introduction to Infrared and Raman Spectroscopy, Academic Press, New York, 1975.
[58] C.Y. Panicker, H.T. Varghese, K.C. Mariamma, K. John, S. Mathew, J. Vinsova, C. Van Alsenoy, Y.S. Mary, J. Raman Spectrosc. 41 (2010) 707–716.
[59] Z.H. Chohan, M.H. Youssoufi, A. Jarrahpour, T.B. Hadda, Eur. J. Med. Chem. 45 (2010) 1189–1199.
[60] A. Hangen, A. Bodoki, L. Orpean, G. Alzuet, M. Liu-Gonzalez, J. Borras, Polyhedron 29 (2010) 1305–1313.
[61] H.T. Varghese, C.Y. Panicker, P.L. Anto, D. Philip, J. Raman Spectrosc. 37 (2006) 487–491.
[62] A. Cravino, H. Neugebauer, S. Luzzati, M. Catellani, N.S. Sariciftci, J. Phys. Chem. 105B (2001) 46–52.
[63] J. Coats, R.A. Meyers (Eds.), Encyclopedia of Analytical Chemistry: Interpretation of Infrared Spectra, A Practical Approach, John Wiley & Sons, Chichester, 2000.
[64] G. Varsanyi, Assignments for Vibrational Spectra of Seven Hundred Benzene Derivatives, Wiley, New York, 1974.
[65] A. Dandia, P. Sarawgi, M.B. Hursthouse, A.L. Bingham, M. Elight, J.E. Drake, R. Ratnani, J. Chem. Res. (July 2006) 445–448.
[66] R.N. Jadeja, J.R. Shah, E. Suresh, P. Paul, Polyhedron 23 (2004) 2465–2474.

[67] E. Lasibal, I. Rodriguez, A. Sousa-Pedraves, M. Alonso, A. Vizoso, J. Romero, J.A. Garcia-Vazquez, A. Sousa, J. Organomet. Chem. 691 (2006) 1321–1392.
[68] C.H. Endredi, F. Billes, S. Holly, J. Mol. Struct. Theochem. 633 (2003) 73–82.
[69] G. Tamasi, L. Chiasserini, L. Zavini, A. Sega, R. Cini, J. Inorg. Biochem. 99 (2005) 1347–1359.
[70] D.A. Kleinman, Phys. Rev. 126 (1962) 1977–1979.
[71] M. Adant, L. Dupuis, L. Bredas, Int. J. Quantum. Chem. 56 (2004) 497–507.
[72] J.S. Murray, K. Sen, Molecular Electrostatic Potentials, Concepts and Applications, Elsevier, Amsterdam, 1996.
[73] J.M. Seminario, Recent Developments Applications of Modern Density Functional Theory, vol. 4, Elsevier, 1996, pp. 800–806.
[74] N. Okulik, A.H. Jubert, Internet Electron. J. Mol. Des. 4 (2005) 17–30.
[75] R.G. Parr, L.V. Szentpaly, S.J. Liu, Am. Chem. Soc. 121 (1999) 1922–1924.
[76] P.K. Chaltraj, B. Maiti, U.J. Sarbar, J. Phys. Chem. A 107 (2003) 4973–4975.
[77] R.G. Parr, R.A. Donnelly, M. Levy, W.E. Palke, Am. Chem. Soc. 68 (1978) 3801–3807.
[78] R. Parthasarathi, J. Padmanabhan, V. Subramanian, B. Maiti, P.K. Chattraj, J. Phys. Chem. A 107 (2003) 10346–10352.
[79] J. Choo, S. Kim, H. Joo, Y. Kwon, J. Mol. Struct. (Theochem.) 587 (2002) 1–8.